

The Nature of Laves Phases: An Explorative Investigation of the Nb-Co System

Daniel Grüner, Frank Stein¹, Martin Palm¹, Joachim Konrad¹, Tadahiro Yokosawa², Alim Ormeci, Walter Schnelle, Osamu Terasaki², Yuri Grin, and Guido Kreiner

Laves phases have the general composition AB_2 and form one of the largest groups of intermetallic compounds with more than 1400 known examples. They crystallize in three structure types: cubic $MgCu_2$ (C15), hexagonal $MgZn_2$ (C14) and hexagonal $MgNi_2$ (C36). In the first half of the last century it was shown in the pioneering works of J. B. Friedauf [1,2], F. Laves [3,4], G. E. R. Schulze [5], F. C. Frank and J. S. Kasper [6,7], that the Laves phases can be regarded as tetrahedrally close packed structures of components A and B with tetrahedral interstices only. The ideal ratio of the radii, based on a hard-sphere model, is $r_A/r_B = \sqrt{3/2}$ with two kinds of coordination type polyhedra. The Frank-Kasper polyhedron Z16 surrounding the A atoms has 4 six-fold A vertices and 12 five-fold B vertices, whereas the icosahedron surrounding the B atoms has 6 five-fold A and 6 five-fold B vertices. The structure types C15, C14 and C36 can be regarded as polytypes with c_3 , h_2 , and $(ch)_2$ stacking sequences in Jagodzinski-Wyckoff notation [8] of one common slab composed of tetrahedra and truncated tetrahedra [9]. The A atoms form a four-connected network interpenetrated by a six-connected network of the B atoms. Approximately 25% of the binary Laves phases exhibit considerable homogeneity ranges [10].

Laves phases have been studied intensely to understand the fundamental aspects of phase stability. However, simple factors governing the crystal

structure type of geometric (r_A/r_B) and electronic (valence electron concentration, vec , and electronegativity difference, $\chi_A - \chi_B$) nature have proven to be helpful in predicting the occurrence and stability of the Laves phases in strictly limited cases [11, 12] only. In general, phase stability and properties of Laves phases are difficult to forecast, especially the origin of the homogeneity ranges and disorder phenomena.

In order to understand the nature of Laves phases, studies on a number of Nb-TM alloy systems with $TM = Cr, Mn, Fe$ and Co are in progress by combining experimental and theoretical methods. Since January 2006 this work is part of an inter-institutional research initiative of the Max Planck Society with the Max Planck Institutes for Metals Research and for Solid State Research in Stuttgart, the “Max-Planck-Institut für Eisenforschung” in Düsseldorf and the Max Planck Institute for Chemical Physics of Solids in Dresden as members. The results discussed here are based on the preparatory work [13-17] related to the proposal of the project.

The binary system Nb-Co is particularly suitable to throw light on the stability of the polytypes due to the coexistence of the C14, C15 and C36 Laves phases. The homogeneity ranges of the Laves phases

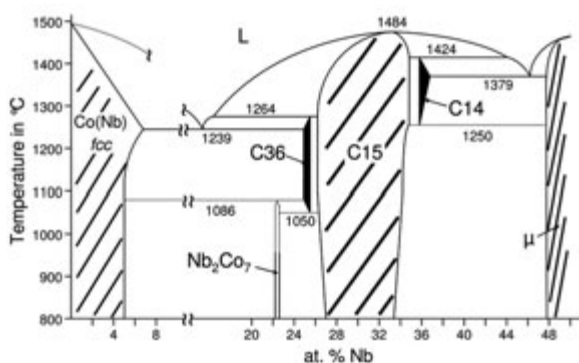


Fig. 1: Schematic phase equilibria in the Nb-Co phase diagram (0 – 50 at. % Nb).

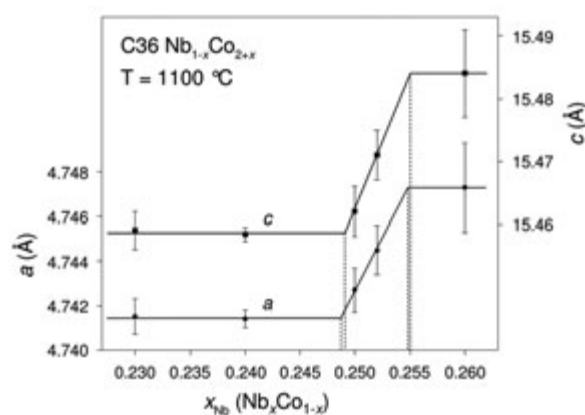


Fig. 2: Unit cell parameters a and c of the hexagonal C36 $Nb_{1-x}Co_{2+x}$ phase vs. composition. Phase boundaries at the annealing temperature 1100 °C are given by dashed lines.

es in this system were determined by phase analyses of samples annealed at appropriate temperatures and by applying the diffusion couple technique. A schematic section of the Nb–Co phase diagram is shown in Fig. 1. The C36 and the C14 phases form strongly off-stoichiometric at lower and higher Nb concentration, respectively, and only at high temperatures. Both phases exhibit a small homogeneity range while the room temperature phase C15 shows a large asymmetrical homogeneity range enclosing the stoichiometric composition NbCo₂.

The Laves phase Nb_{1-x}Co_{2+x} with C36 structure type forms close to the composition NbCo₃ with a narrow homogeneity range from 24.8(5) to 25.5(5) at.% Nb. A plot of the unit cell parameters *a* and *c* of the C36 Nb_{1-x}Co_{2+x} phase vs. the composition is shown in Fig. 2. The temperature range of

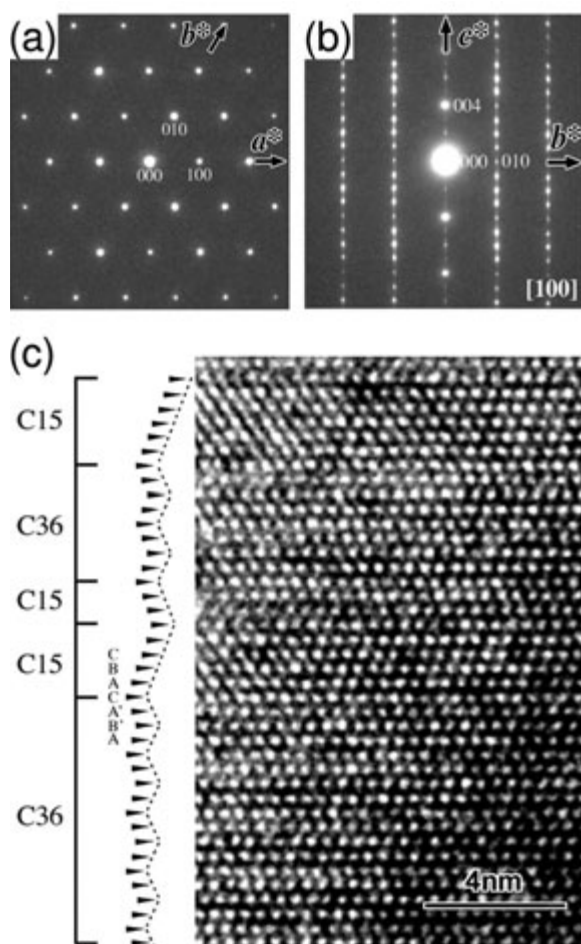


Fig. 3: Real crystal structure of C36 (Nb_{0.759}Co_{0.241})Co₂ obtained from a sample containing a mixture of C36 and C15 phases. SAED patterns along [001] (a) and [100] (b). (c) HREM image along [100] displaying stacking faults with stacks of C15 sequence.

the phase field is limited by an eutectoid (C36 = Nb₂Co₇ + C15) and a peritectic (L + C15 = C36) reaction at ≈1050°C and 1264°C, respectively. The width of the two-phase field C36 + C15 is smaller than 1 at.%. A sample containing a mixture of C15 and C36 phases was investigated by transmission electron microscopy. Selected area electron diffraction (SAED) patterns (Fig. 3a and 3b) of the C36 phase reveal diffuse streaks along the *c**-direction. This suggests the existence of stacking faults perpendicular to the *c*-direction — at least for Nb-rich C36 Nb_{1-x}Co_{2+x}. Such stacking faults are shown in a corresponding HREM image in Fig. 3c. The off-stoichiometry is caused by a random substitution of ≈25% of the Nb atoms by additional Co atoms. Neither vacancies at Nb sites nor Co atoms at interstitial sites have been detected, ditto an ordered superstructure was not observed. The excess Co atoms occupy preferentially one of two crystallographic Nb sites. Twice as much Co substitutes the Nb2 site as compared to the Nb1 site.

The crystal structure exhibits pronounced deviations from an idealized crystal structure with structural parameters taken from the hard sphere model for the Co and the Nb network. A part of the Co network composed of Co₄ tetrahedra (linked by common vertices in case of Co₂Co₃ and common triangular faces in case of Co₁Co₃) is shown in Fig. 4a. A three-layer stack of hexagonal sequence Co3–Co1–Co3 is shown in Fig. 4b. The Kagomé

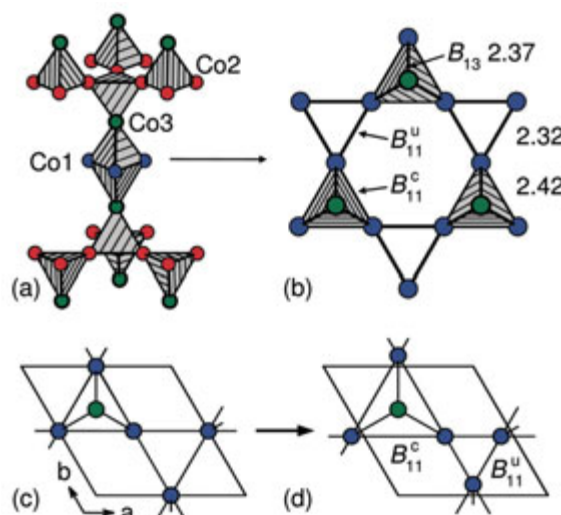


Fig. 4: The Co network of C36 Nb_{1-x}Co_{2+x} at *x* = 0.265. (a) Part of the Co network including three Kagomé and four triangular layers. (b) Hexagonal arrangement of three sequential layers. (c) and (d) Schematic illustration of the distortion pattern of the Co1 Kagomé layers.

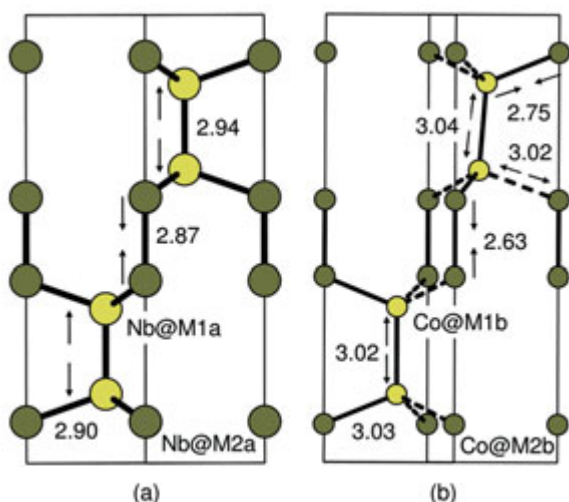


Fig. 5: Distortion of the Nb network of C36 Nb_{1-x}Co_{2+x}, $x = 0.265$. The distortions are indicated by arrows and the interatomic distances are given in Å. (a) Nb@M1a and Nb@M2a. b) Co@M1b and Co@M2b.

layers of the hexagonal slab display an elongation of the edges (B_{11}^c) of the basal triangles of the Co₁₃Co₃2 trigonal bipyramids and a contraction of the edges (B_{11}'') of the uncapped triangles. The distortion pattern of the hexagonal slabs is illustrated in Figs. 4c and 4d. This type of distortion with $B_{11}'' < B_{13} < B_{11}^c$ is in agreement with the one found for the majority of C14 and C36 Laves phases whose atomic positions have been refined.

The Nb network of C36 Nb_{1-x}Co_{2+x} is a four-connected net of 4H-SiC (carborundum III) topology and shows pronounced deviations from regularity. It may be described as a sequence of double layers equivalent to {Nb2 Nb2}–{Nb1 Nb1}–{Nb2

Nb2}–{Nb1 Nb1} per unit cell, and labels Nb1, Nb2 denote the two different crystallographic Nb sites in the idealized crystal structure. Upon distortion, three different interatomic distances $d(M1a-M1a) = 293.5$ pm, $d(M2a-M2a) = 286.5$ pm, and $d(M1a-M2a) = 290.2$ pm with M1a and M2a labeling Nb1 and Nb2 shifted from the positions of the idealized crystal structure are generated. The distance $d(M1a-M1a)$ is elongated, $d(M2a-M2a)$ shorter and $d(M1a-M2a)$ equal compared to $d(Nb-Nb) = 290.2$ pm of the model without distortion. A schematic illustration of the distortion of the Nb network is shown in Fig. 5a.

The random substitution of approx. 25% of all Nb atoms by the smaller Co atoms triggers a local displacement of the Co atoms on Nb sites. These positions are labelled here M1b and M2b. The split atom positions (M1a, M1b) and (M2a, M2b) correspond to distinct maxima in the difference electron density contour maps as shown in Fig. 6. The electron density obtained from X-ray single crystal structure refinements at M1 = (M1a, M1b) is a trigonal pyramid with Nb@M1a at the apical position and a dumbbell at M2 = (M2a, M2b). A snapshot of the Co@Nb network assuming 100% substitution is shown in Figure 5b. Random substitution, preferred occupation of the Nb2 site by Co, and displacements of Co relative to Nb atoms make the real structure exceedingly complicated. The main factor for the displacement of the Co atoms at the Nb network is the formation of Co–Nb pairs with interatomic distances comparable to those between Co and Nb atoms of the respective networks. According to measurements of the magnetization

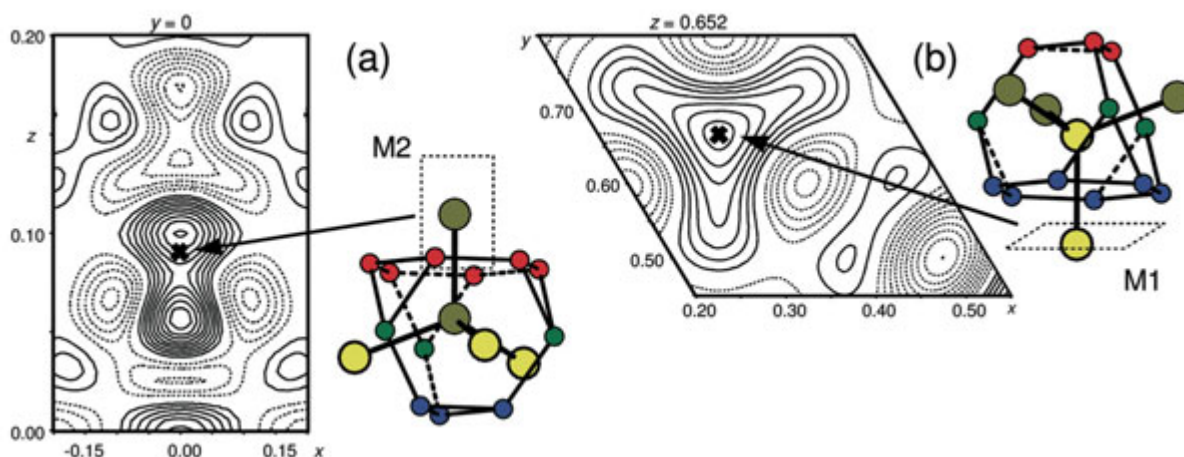


Fig. 6: Difference electron density maps around the M2 (a) and M1 (b) sites. Position and alignment for both regions within the crystal structure are indicated by the dashed line. Crosses mark the idealized position of Nb.

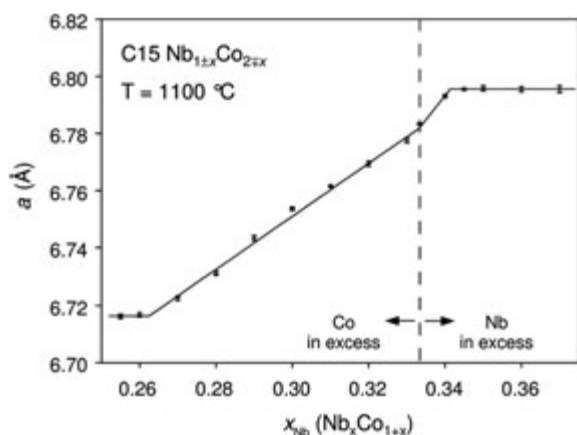


Fig. 7: Plot of unit cell parameters a of the cubic C15 phase vs. composition. The ideal composition is indicated by the dashed line.

and the electrical resistivity of a single phase sample C36 $\text{Nb}_{0.735(1)}\text{Co}_{2.265}$ is Pauli paramagnetic with larger residual resistivity compared to C15 NbCo_2 indicating significant structural disorder in the former compound.

The C15 polytype crystallizes at 1100 °C in the range from 26.2 to 34.5 at.% Nb and melts congruently at 1484 °C. Single-phase material has been obtained from 28 to 34 at.% in steps of 1 at.%. The unit cell parameter a follows Vegard's rule on the Co-rich side which is shown in Fig. 7. Here, the origin of the homogeneity range is due to excess Co randomly occupying Nb positions, a fact shown by single crystal structure investigations in combination with chemical analyses. No conclusive information for the Nb-rich side is so far available. The C15 Laves phase is a metal with Pauli paramagnetic behaviour. Specimens of the C15 phase obtained from the C36 + C15 and from the C15 + C14 two phase fields have been investigated by means of SAED, HREM and convergent beam electron diffraction (CBED) techniques. The findings confirm the space group $Fd\bar{3}m$ and no superstructure reflections have been observed. Stacking faults for the Co-rich C15 phase were rarely observed while Nb-rich C15 specimens often exhibited stacking faults.

The homogeneity range of C14 $\text{Nb}_{1+x}\text{Co}_{2-x}$ extends from 36.3(2) to 37.2(2) at.% Nb at 1280 °C according to EPMA measurements of diffusion couples while at 1350 °C the range is wider: from 36.2(2) to 37.8(2). There is strong evidence supported by chemical analyses of homogenized samples as well as results obtained from structure refinements that the above values are shifted 0.5 to

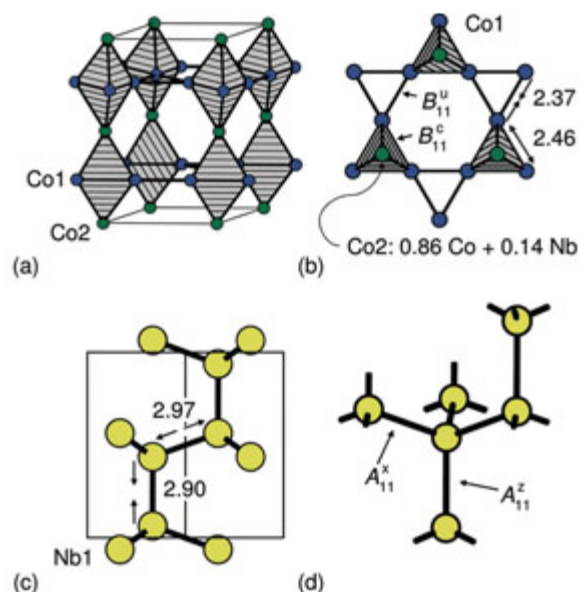


Fig. 8: The Co and Nb network of C14 $\text{Nb}_{1+x}\text{Co}_{2-x}$ at $x = 0.07$. The interatomic distances are given in Å and the labels denote the different bond types. (a) Part of the Co network including two Kagomé and three triangular layers. (b) Hexagonal arrangement of three sequential layers. (c) and (d) Part of the Nb network.

1.0 at.% to higher Nb concentrations due to a systematic error of the EPMA measurements. The phase width probably increases until the C14 phase participates in a eutectic reaction ($L = \text{C14} + \mu$) at 1379 °C. On the Co-rich side C14 forms a very narrow two-phase field (≈ 1 at.%) together with the C15 phase. The C14 phase forms in a peritectic reaction from C15 and a liquid phase at 1425 °C ($L + \text{C15} = \text{C14}$). At lower temperatures, the phase field is bounded by a eutectoid reaction at ≈ 1250 °C ($\text{C14} = \text{C15} + \mu$). However, the reaction is too sluggish to be observed in DTA measurements. The off-stoichiometry is caused by a random substitution of approx. 14% Co by Nb atoms at one of the two crystallographically independent Co sites (Co2 in Fig. 8a) according to single crystal structure and Rietveld powder profile refinements. Vacancies at Co sites, Nb atoms at interstitial sites, or an ordered superstructure have not been detected. The Co and the Nb networks are both distorted with respect to the idealized crystal structure of C14 NbCo_2 based on the hard sphere model. The Co network of the C14 phase reveals a similar distortion pattern (see Fig. 4c and 4d) as that of the C36 phase. The distortion is again characterized by a contraction of the edges of uncapped triangles (B_{11}^u) and an expansion of the edges of the basal triangles (B_{11}^c) of

the trigonal bipyramids Co_3Co_2 , as shown in Fig. 8b.

The Nb network of $\text{C14 Nb}_{1+x}\text{Co}_{2-x}$ is a four-connected net of 2H-ZnS (wurtzite) topology and shows pronounced deviations from regularity. It may be described as a sequence of double layers equivalent to $\{\text{Nb1 Nb1}\}-\{\text{Nb1 Nb1}\}$ per unit cell as shown in Fig. 8c. Upon distortion, two different interatomic distances $d(\text{Nb1-Nb1}) = 297.2$ pm and $d(\text{Nb1-Nb1}) = 290.2$ pm arise, one longer, the other one shorter than the shortest Nb-Nb distance of 295.4 pm of the undistorted model.

In order to study the distortion of the Co and the Nb network, the preferential substitution of different crystallographic Nb or Co sites, and — in case of the C36 phase — the local displacement of Co at Nb sites, electronic structure calculations have been performed by TB-LMTO-ASA and full potential methods (FPLO) [18,19]. Since the crystal structures of both phases are strongly disordered, stoichiometric C36 and C14 NbCo_2 as well as appropriate ordered superstructures have been used as models. The following conclusions can be drawn from the results of the calculations:

- The idealized crystal structures of C14 and C36 at stoichiometric composition NbCo_2 obtained from the hard sphere model should be unstable with respect to a distortion of the Co and the Nb network according to the full potential total energy calculations. The distortion patterns obtained by the calculations for C36 and C14 NbCo_2 are similar to the observed distortion patterns for off-stoichiometric compositions:

$$\text{C36: } B_{11}^u < B_{13} \approx B_{22} \approx B_{23} < B_{11}^c \text{ and}$$

$$A_{22} < A_{12} < A_{11}$$

$$\text{C14: } B_{11}^u < B_{12} < B_{11}^c \text{ and } A_{11}^z < A_{11}^x$$

- For a discussion of the influence of the off-stoichiometry, i.e. excess Co or Nb, on the distortion more detailed investigations and calculations are needed.
- Total energy calculations for the C36 phase predict that the substitution of Nb2 by Co is energetically slightly more favorable compared to a substitution of Nb by Co at Nb1. However, the difference in energy is very small allowing for disorder at both sites. In case of the C14 phase, the substitution of Co by Nb atoms at Co2 (triangular layers) is energetically preferred compared to a substitution of Co at Co1 by Nb. So far the origin of the differences in the total energy in terms of a local bonding picture is unknown.

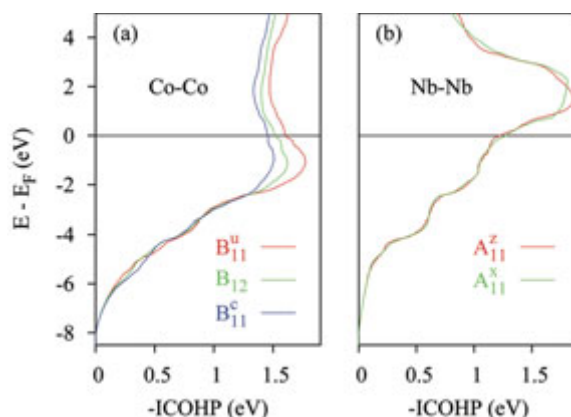


Fig. 9: Integrated crystal orbital Hamilton population curves ($-\text{ICOHP}$) for the different types of bonds within C14 NbCo_2 with idealized structural parameters obtained from the hard sphere model. (a) Co-Co; (b) Nb-Nb.

However, in case of the C36 phase the preferential occupation of Co at the Nb2 site must be due to medium or long range interactions since the atomic environment for both Nb sites is equal up to the third coordination shell.

- The local displacement of Co at Nb sites originates from a formation of a small number of Co-Nb pairs with interatomic distances comparable to that between Co and Nb in stoichiometric NbCo_2 (≈ 2.70 Å).
- Assuming that the integrated crystal orbital Hamilton population ($-\text{ICOHP}(E_F)$) values obtained from LMTO-ASA calculations can be used as a measure of bond strength, the non-uniform bond strength distribution for the Co network in all models may be interpreted as a tendency towards distortion. As an example, a plot of the $-\text{ICOHP}(E)$ for Co-Co and Nb-Nb for idealized C14 NbCo_2 is shown in Fig. 9. The $-\text{ICOHP}(E_F)$ for Co-Co bonds are clearly different although all interatomic distances $d(\text{Co-Co})$ for nearest neighbors are equal in this model.
- A similar correlation does not hold for the Nb-Nb bonds in the Nb network.

References

- [1] J. B. Friauf, J. Am. Chem. Soc. **49** (1927) 3107.
- [2] J. B. Friauf, Phys. Rev. **29** (1927) 34.
- [3] F. Laves and H. Witte, Metallwirtschaft **14** (1935) 645.
- [4] F. Laves and H. Witte, Metallwirtschaft **15** (1936) 840.
- [5] G. E. R. Schulze, Z. Elektrochem. **45** (1939) 849.

- [6] *F. C. Frank and J. S. Kasper*, *Acta Crystallogr.* **11** (1958) 184.
- [7] *F. C. Frank and J. S. Kasper*, *Acta Crystallogr.* **12** (1959) 483.
- [8] *H. Jagodzinski*, *Acta Crystallogr.* **7** (1954) 17.
- [9] *S. Samson*, *Development in the Structural Chemistry of Alloy Phases*, *B. C. Giessen* (ed.), Plenum Press, New York, 1969.
- [10] *D. J. Thoma and J. H. Perepezko*, *J. Alloys Compd.* **224** (1995) 330.
- [11] *F. Stein, M. Palm and G. Sauthoff*, *Intermetallics* **12** (2004) 713.
- [12] *F. Stein, M. Palm and G. Sauthoff*, *Intermetallics* **13** (2005) 1056.
- [13] *D. Grüner, A. Ormeci, G. Kreiner, and Y. Grin*, *Z. Anorg. Allg. Chem.* **630** (2004) 1725.
- [14] *D. Grüner, G. Kreiner and Y. Grin*, *Z. Kristallogr. (Supplement)* **21** (2004) 159.
- [15] *D. Grüner, F. Stein, M. Palm, J. Konrad, A. Ormeci, W. Schnelle, Y. Grin, and G. Kreiner*, *Z. Kristallogr.*, in press.
- [16] *T. Yokosawa, K. Söderberg, M. Boström, D. Grüner, G. Kreiner, and O. Terasaki*, *Z. Kristallogr.*, in press.
- [17] *D. Grüner, F. Stein, M. Palm, A. Ormeci, Y. Grin, and G. Kreiner*, submitted to *Z. Anorg. Allg. Chem.*
- [18] *G. Krier, O. Jepsen, A. Burkhard and O. K. Andersen*, *Tight Binding LMTO-ASA Program, Version 4.7*, Stuttgart, Germany 1998.
- [19] *K. Koepernik and H. Eschrig*, *Phy. Rev.* **B59** (1999) 1743.

¹ Max-Planck-Institut für Eisenforschung GmbH, Düsseldorf, Germany

² Arrhenius Laboratory, Stockholm University, Stockholm, Sweden